A&A manuscript no.	<u> </u>
(will be inserted by hand later)	ASTRONOMY
Your thesaurus codes are: ()	AND ASTROPHYSICS 27.8.2018

Calcium Triplet Synthesis

M.L. García-Vargas^{1,2}, Mercedes Mollá^{3,4}, and Alessandro Bressan⁵

- Villafranca del Castillo Satellite Tracking Station. PO Box 50727. 28080-Madrid, Spain.
- ² Present address at GTC Project, Instituto de Astrofísica de Canarias. Vía Láctea S/N. 38200 LA LAGUNA (Tenerife)
- ³ Dipartamento di Fisica. Università di Pisa. Piazza Torricelli 2, I-56100 -Pisa, Italy
- ⁴ Present address at Departement de Physique Université Laval. Chemin Sainte Foy . Quebec G1K 7P4, Canada
- ⁵ Osservatorio Astronomico di Padova. Vicolo dell' Osservatorio 5. I-35122 -Padova, Italy.

Received xxxx 1997; accepted xxxx 1998

Abstract. 1

We present theoretical equivalent widths for the sum of the two strongest lines of the Calcium Triplet, CaT index, in the near-IR ($\lambda\lambda$ 8542, 8662 Å), using evolutionary synthesis techniques and the most recent models and observational data for this feature in individual stars.

We compute the CaT index for Single Stellar Populations (instantaneous burst, standard Salpeter-type IMF) at four different metallicities, Z=0.004, 0.008, 0.02 (solar) and 0.05, and ranging in age from very young bursts of star formation (few Myr) to old stellar populations, up to 17 Gyr, representative of galactic globular clusters, elliptical galaxies and bulges of spirals. The interpretation of the observed equivalent widths of CaT in different stellar systems is discussed.

Composite-population models are also computed as a tool to interpret the CaT detections in star-forming regions, in order to disentangle between the component due to Red Supergiant stars, RSG, and the underlying, older, population. CaT is found to be an excellent metallicity-indicator for populations older than 1 Gyr, practically independent of the age. We discuss its application to remove the age-metallicity degeneracy, characteristic of all studies of galaxy evolution based on the usual integrated indices (both broad band colors and narrow band indices). The application of the models computed here to the analysis of a sample of elliptical galaxies will be discussed in a forthcoming paper (Gorgas et al. 1997).

Key words: Spectroscopic indices – Stellar Populations — Calcium Triplet – Cool stars – Starbursts — Elliptical galaxies

1. Introduction

The Ca II triplet in absorption, at $\lambda\lambda$ 8498, 8542, 8662 Å, is the strongest feature in the near-infrared spectrum of late-type stars and normal galaxies. Pioneer work by Jones *et al.* (1984) was followed by those of Díaz *et al.* (1989, hereafter DTT89), Zhou (1991, hereafter Z91) and Mallik (1994), who studied the behaviour of these features in several stellar libraries, as a function of the atmospheric stellar parameters: effective temperature, $T_{\rm eff}$, surface gravity, logg, and iron abundance, [Fe/H].

DTT89 observed a sample of 106 late-type stars (up to K5III) in the near-IR, providing the first homogeneous atlas including CaT. They defined standard spectral windows, free of TiO contamination, to locate the continuum

Send offprint requests to: M.L. García-Vargas

Tables 1 to 10 are only available in electronic form at CDS via an onymous ftp to cdsarc.u-strasbg.fr (130.79.128.5) or via http://cdsweb.u-strasbg.fr/Abstract.html

and to measure the index. They concluded that the equivalent width of the two main lines ($\lambda\lambda$ 8542, 8662 Å) of the Ca II triplet, EW(CaT), increases with increasing metallicity and decreasing stellar surface gravity of the star and, at high metallicity ($Z \ge 0.5 Z_{\odot}$), the surface gravity is the dominant parameter, with values of EW(CaT) larger than 9 Å found only in RSG. This behaviour was later confirmed by Z91 and Mallik (1994).

Zhou reached the same conclusions that DTT89 but adopting slightly different spectral windows for the index definition. The analysis of the values of the EW(CaT) for the stars in common allow us to combine both atlases. In particular, Z91 includes M-late giant stars, not present in DTT's library. For these M giants, it appears that the correlation between EW(CaT) and T_{eff} is stronger than that between EW(CaT) and log g. Z91 shows that in M giants EW(CaT) reaches values lower than the ones predicted only on the basis of the EW-logg calibration previously found by DTT89.

Mallik (1994) observed 91 late-type stars, confirming the results of DTT89 and Z91. The lack of the measurement of the 8662 Å line for a large part of his sample and the different continuum band-passes and spectral resolution, make very difficult the comparison between Mallik's atlas and those of DTT89 and Z91. Mallik's sample does not include stars cooler than M1, and therefore no conclusions about the values of the index for extremely cool stars can be achieved. However, for the coolest stars in this atlas the values of EW(CaT) are lower for lower T_{eff}, confirming the T_{eff}-dependence of the index for the coolest stars.

Recently, Idiart et al. (1997) have published CaT indices for a sample of 55 stars. Their sample do not include cool M stars neither metal-rich supergiant stars. The cool late-type stars are however included in their calibration since they use those from Z91 (converting the values of CaT given by Z91 to their own system). The definition of their indices is different from the one assumed in this work (common in DTT89 and Z91): they used different continuum band-passes and the three CaT lines (instead of the two strongest ones), being the comparison meaningless. Nevertheless, they confirm the strong dependence on metallicity. With respect to the T_{eff} -dependence, they find that the strength of CaT increases from F2 to K5 stars.

From the theoretical point of view, Smith & Drake (1987; 1990) and Erdelyi-Mendes & Barbuy (1991) computed the intensities of CaT lines, as a function of the atmospheric parameters ($T_{\rm eff}$, logg and metallicity). These last authors found that the computed intensity of CaT lines increases exponentially with metallicity (DTT89 had found a linear relation but in a narrower range of metallicities), showing a stronger dependence on metallicity when gravity is low (giant and supergiant stars). They also found a weak dependence on effective temperature and a modest dependence on gravity.

Finally, Jørgensen et al. (1992; hereafter JCJ92) computed a complete grid of models for Ca II lines as a function of T_{eff}, logg and [Ca/H] abundance. They synthesized the equivalent widths of CaT lines. They used the DTT89 index definition and therefore compared these results with the published observational data. They found a good agreement between their calibrations and the observed EW(CaT) compiled by DTT89, reaching basically the same conclusions already pointed out, that can be summarized as follows: (1) in high metallicity systems, the stellar surface gravity is the parameter which controls the strength of the CaT lines; (2) the effect of the abundance is very important for giants and supergiants, with EW(CaT) increasing at increasing metallicity, but not for dwarfs; (3) at lower metallicity the effect of the effective temperature is in competition with that of the gravity.

In the present work we compute stellar population synthesis models for the sum of the equivalent widths of the two strongest lines ($\lambda\lambda$ 8542, 8662 Å) of the CaT. The age considered ranges from 1 Myr to 13 Gyr, and the metallicity from 0.2 Z_{\odot} to 2.5 Z_{\odot} . Section 2 describes the main aspects of the evolution related to the appearance of cool stars on the basis on the Padova evolutionary tracks (2.1), and the computed Spectral Energy Distributions, SEDs, in which both, stellar (2.2) and nebular (2.3) contributions have been included. Section 3 is devoted to the CaT synthesis. Two grids of models have been computed: grid I which is based on the theoretical fitting functions of EW(CaT) (section 3.1), and grid II, based on empirical fitting functions derived from the above stellar atlases (section 3.2).

In addition to the models described in section 3, several composite-population models have been computed with different mass percentages of young (2.5 - 5 Myr), able to ionize), intermediate (8 - 12 Myr), rich in RSG) and very old (10 Gyr) populations. These models are described in section 4.1 and are meant to constitute a reference frame for the interpretation of the observations of CaT in star-forming regions at different scales (from pure HII regions to Starburst galaxies or even Active Galactic Nuclei, AGN). Section 4.2 discusses the implications of the use of CaT as a metallicity indicator in elliptical galaxies. Finally, section 5 summarizes the conclusions.

2. Evolutionary Synthesis Models

We have computed models for Single Stellar Populations (instantaneous burst), at four different metallicities ($Z = 0.2 Z_{\odot}$, $0.4 Z_{\odot}$, Z_{\odot} and $2.5 Z_{\odot}$, and ranging in age between 1 Myr (logt = 6.00) and 13 Gyr (logt = 10.12), with a

logarithmic step in age (given in years) of 0.1. The model at 17 Gyr was also computed to compare with other authors (see section 4.2 and Figure 6).

The total mass of the SSP is $1 \times 10^6 \,\mathrm{M}_\odot$ with a Salpeter-type IMF (Salpeter 1955), $\phi(m) = m^{-\alpha}$, $\alpha = 2.35$, from the lower limit $m_{low} = 0.8 \,\mathrm{M}_\odot$ to the upper limit $m_{up} = 100 \,\mathrm{M}_\odot$. Taking into account the Padova evolutionary tracks (see section 2.1), a fine grid of isochrones has been computed following the method outlined by Bertelli *et al.* (1994). We also synthesized a complete grid of isochones with $m_{low} = 0.6 \,\mathrm{M}_\odot$ to check the effect of considering a lower limit of the IMF on CaT index, finding a maximum discrepancy of 10 % and only for ages older than 4 Gyr.

Once the HR Diagram is calculated and the SED for the SSP computed (see sections 2.2, 2.3), we are able to calculate the EW(CaT) in the integrated populations by taking the EW(CaT) of individual stars from theoretical models (JCJ92), or observed stellar libraries (DTT89, Z91) as will be outlined in section 3.

2.1. Stellar Evolution

Isochrones were constructed at several ages by interpolating between the evolutionary sequences calculated by Bressan et al. (1993), and Fagotto et al. (1994a,b). These tracks were computed using the radiative opacities of Iglesias et al. (1992) for the initial chemical compositions Z=0.004, Y=0.24; Z=0.008, Y=0.25; Z=0.02 and Z=0.05, Y=0.352 (Padova models).

Recent reviews on stellar evolution can be found in Maeder & Conti (1995) and Chiosi et al. (1992). Here we will briefly summarize the main properties of the adopted models, with particular emphasis to the red giant and red supergiant phases which are the most relevant to the CaT synthesis.

Red giant stars appear suddenly after hydrogen in the center has been exhausted. Two remarkable exceptions are constituted by the most massive stars if mass-loss is strong enough to peal-off the envelope of the star thus avoiding the expansion phase, and by stars around $20~\rm M_{\odot}$ if the mixing criterion in the intermediate convective shell and in the previous H-burning core is such that the model ignites and burns He in the center as a yellow supergiant star (case A evolution, usually associated with the Schwarzschild criterion for the convective instability, Deng et al. 1996). For all the other initial masses the models possess a red giant phase of significant duration. Old clusters with turn-off mass, M_{Toff} , lower than $2~\rm M_{\odot}$, have a well populated red giant branch (RGB). For a sufficient high metallicity and/or relatively young age these clusters also show a red clump of He-burning stars tied to the RGB. On the contrary, in intermediate-age and young clusters, only the red clump of He-burning stars is populous and luminous enough to have observable effects. Usually for a sufficiently high initial mass and low metal content part of the central He is burnt in a blue loop toward higher effective temperatures. Finally old and intermediate age clusters, $M_{Toff} < 5$ -6 M_{\odot} , also display the asymptotic giant branch (AGB) phase. The fuel consumed in this phase is relatively high so that the contribution to the integrated light is not negligible.

As already anticipated the evolution of the most massive stars is still unclear because of our poor knowledge of the efficiency of internal mixing processes and of the mass-loss phenomenon. The Padova models account for mild overshoot from the convective core, and mass loss by stellar winds has been accounted for according to the rates given by de Jager et al. (1988) from the main sequence up to the so-called de Jager limit in the HRD. Beyond the de Jager limit the most massive stars enter the region where Luminous Blue Variables (LBV) are observed and, accordingly, the mass-loss rate has been increased to $10^{-3} M_{\odot} \text{ yr}^{-1}$. As the evolution proceeds, the surface hydrogen abundance by mass in the most massive stars eventually falls below the value of 0.3. In this case the model is supposed to become a Wolf-Rayet (WR) star and the mass-loss rate is derived according to Langer (1989).

As a matter of fact there are several unsolved questions in the HR diagram of the most massive stars, among which we recall the existence of the so called blue Hertzsprung gap, a region where, contrary to what is observed, theory predicts a negligible number of stars; the observational evidence of the de Jager limit at the highest luminosities, which is reproduced by the models only by adopting an arbitrarily high mass-loss rate (of the order of $10^{-3} M_{\odot}/\text{yr}$) in the corresponding region of the HR diagram; and finally the problem of the Wolf-Rayet stars, which are either much cooler or less luminous than predicted by the models. Nevertheless the theory predicts that massive stars with initial mass between 10 and 30 solar masses, spend a significant fraction ($\simeq 50\%$) of their He burning phase as red supergiant but the effective temperature of these stars is a matter of debate, and this must be reminded when assigning the spectral type during the synthesis process. In general the effective temperature predicted by the theory is higher than what is observed, but one must bear in mind that the majority of the models adopt a static gray atmosphere as a boundary condition, while that of RSG stars is an extended and expanding atmosphere. Moreover the suppression of the density inversion or the adoption of a density scale-height in the convective envelope, both result into a higher effective temperature (Bressan et al. 1993). Finally RSG are losing mass at a rate of about $10^{-5} M_{\odot}/\text{yr}$ and dust processes in the circumstellar envelope can also affect their color and then their apparent location in the HR diagram.

Another important question is whether a young SSP may contain RSG and WR stars at the same time. Bressan (1994) and García-Vargas et al. (1995a) have shown that this is marginally possible for an age of 6 Myr and Z=0.02. In fact in our standard view, WR stars evolve in the HR diagram from the highest luminosities almost vertically downward and thus their presence is associated with very young ages. RSG on the contrary, only appear after a few Myr have elapsed from the burst onset. However Bressan (1994) showed that by adopting the mass-loss parameterization of de Jager et al. (1988), the predicted mass-loss rate of a typical RSG model of 20 M_{\odot} of solar composition is significantly lower than that derived by means of the Feast formulation (1992), which empirically links the mass-loss rate to the period of pulsation of the RSG stars. Recent models of massive stars of solar composition, in which one adopts the mass-loss formulation by Feast (1992), show that 20 M_{\odot} and 18 M_{\odot} stars leave the RSG phase and enter the main sequence band with a surface hydrogen abundance of 0.43, which is comparable to the one selected by Maeder for the BSG-WNL transition (Salasnich et al. 1997). This "horizontal" evolution into the channel of the low luminosity WR stars allows the presence of WR and RSG stars simultaneously in an instantaneous burst.

Clusters of intermediate age (between 0.1 and 1 Gyr) are characterized by the presence of the very luminous Asymptotic Giant Branch stars (AGB). While their life-time is quite short (around 1 Myr), they are among the brightest stars in the cluster, their fuel consumption is large and their contribution to the integrated light is significant. The appearance of the AGB phase as the SSP evolves is quite sudden at an age of 100 Myr and causes a jump in the colors, in particular when near infrared pass-bands are considered (see eg. Bressan et al. 1994). The same happens to the EW(CaT) in clusters of about 0.1 Gyr (see Fig. 4).

At older ages the contribution of the AGB phase declines while that of the red giant branch (RGB) becomes more and more pronounced. Above 10 Gyr, red giants mainly belong to the RGB phase and the integrated light from the AGB phase has become negligible.

2.2. The Stellar Energy Distributions

We have synthesized the emergent spectrum of an evolving star cluster by calculating the number of stars in each element of the isochrone and assigning to it the most adequate stellar atmosphere model, *i.e.* the closest one in effective temperature and surface gravity. The stellar spectrum has then been scaled to the luminosity of the corresponding theoretical star in the HRD.

To build our stellar spectral library we assembled the stellar atmospheres of Clegg & Middlemass (1987) for stars with $T_{\rm eff} \geq 50000$ K and those of Kurucz (1992) for stars with 5000 K $\leq T_{\rm eff} < 50000$ K. The later models are available at different metallicities. Since the precise shape of the spectrum of the hottest stars does not have any influence in the CaT models presented here, we will not discuss the selected atmosphere models for them (a detailed discussion can be found in García-Vargas 1996 and references therein). For the coolest stars, we have used a blackbody distribution since it can model the level of the continuum at 8600 Å better than Kurucz models (of course the SEDs are not used in any case to synthesize the features, but to locate the continuum level). As an example, Figure 1 shows observed stellar spectra together with the corresponding Kurucz model and blackbody (BB) distribution for some representative spectral types. We have checked quantitatively the differences in the continuum level at 8600 Å between these three representations (BB, Kurucz, and observed) finding a maximum discrepancy of 15 % for the coolest RSG, and only 1 % for giants.

2.3. The Nebular Continuum

Because our aim is to build models that can be applied to star-forming regions, we have computed the continuum nebular emission under the following hypothesis.

The gas is assumed to have an electron temperature, T_e , which is metallicity dependent. The values for T_e = 11000 K (Z= 0.2 Z_{\odot}), 9000 K (Z= 0.4 Z_{\odot}), 6500 K (Z= Z_{\odot}) and 4000 K (Z= 2.5 Z_{\odot}) have been chosen according to the observational determination of T_e in star-forming regions (for the lowest metallicities), and the average value, in the age-range 1.5 - 5.4 Myr, given by photoionization models (García-Vargas et al. 1995b) for the highest Z values. The assumed helium abundance by number is 10 %. The free-free, free-bound emission by hydrogen and neutral helium, as well as the two photon hydrogen-continuum have been included. The atomic data were compiled from Aller (1984) and Ferland (1980) according to the selected value of T_e .

Tables 1 and 2 list the integrated luminosity of the SSPs with different metallicity at some characteristic wavelengths in the UV (2000 Å), optical (4850 Å, representative of the continuum near H_{β}), and infrared (at 2.17 μm , near Br_{γ}). A complete set of tables, including the nebular and stellar contributions separately as well as the total luminosity for our grid of models at wavelengths of 1400, 2000, 4850, 8600 Å, 2.17 and 2.30 μm and the synthetic SEDs are available upon request.

Fig. 1. Comparison between different near-IR spectra of cool stars and stellar atmosphere models. Left panel shows a sequence of giants with effective temperature decreasing from top to bottom. Right panel shows the Red Supergiant sequence. Data (lines with higher spectral resolution) are true stars for the labelled spectral type and luminosity class (Danks and Dennefeld 1994). The degraded spectra correspond to a Kurucz's model of a T_{eff} and logg appropriate for each given star. Finally, the featureless line is the spectral energy distribution of a blackbody whose T_{eff} has been chosen to be equivalent to the assigned Kurucz's model. All the spectra are normalized at 8800 Å

Figure 2 shows the ratio between the nebular and the total luminosity as a function of the age at four selected wavelengths. At Z_{\odot} the nebular contribution in the earliest stages of the burst changes between 20 % in the optical (H_{β}) to almost 90 % in the infrared (2.3 μm). This effect becomes negligible for evolved SSP (older than 5.5 Myr) when the production of ionizing photons is negligible.

However, if a very young (ionizing) burst coexist with a slightly older population (around 10 Myr), RSG rich, such as in the case of some star-forming regions (García-Vargas et al. 1997), the effect of the nebular continuum competes with that of the older stellar component, and some stellar infrared features can be partially diluted. This could be the case of the CO absorption bands at $2.3~\mu m$, where the contribution of the nebular to the total luminosity can be as high as 90%. The same effect also applies to the near-IR colors. For example, if we assume two coexisting populations (one around 2-4 Myr and the other one around 9-12 Myr) contributing with similar percentage in mass, the resulting V-K color would be affected both by the nebular continuum of the young burst and by the stellar continuum from RSG present in the intermediate-age burst. Thus detailed evolutionary synthesis models, using other constraints, would be required in order to correctly interpret the photometric observations.

3. Calcium Triplet Synthesis

We calculate the integrated equivalent widths for the CaT lines by combining the individual stars in each evolutionary stage, according to the theoretical isochrone. To this purpose let I_j be the intensity in absorption of the two lines of CaT for each star, j, found in the HR diagram of an SSP:

$$I_j = f_j E W_j \tag{1}$$

where f_j is the corresponding flux at the wavelength of 8600 Å for the star in the HR diagram. This quantity is obtained by a linear interpolation between the two central values of the continuum band-passes as defined by DTT89. The fluxes come from a suitable stellar atmosphere model and have been scaled to the luminosity of the corresponding



theoretical star in the HR diagram. EW_j is the equivalent width of CaT for a star in the evolutionary stage j, that we assume is known. If N_j describes the number of stars in the evolutionary stage j and N is the total number of points in the HR Diagram, the synthesized equivalent width of CaT for an SSP at a given epoch is:

$$EW(CaT, SSP) = \frac{\sum_{j=1}^{N} I_j N_j}{\sum_{j=1}^{N} f_j N_j + f_{neb}}$$
 (2)

where f_{neb} is the nebular continuum at 8600 Å corresponding to the SSP. In the following both theoretical (grid I) and empirical (grid II) fitting functions have been used to obtain the index as a function of the stellar physical parameters: T_{eff} , logg and abundance. The theoretical stellar grid of EW(CaT) is from JCJ92, while the empirical library is from DTT89 plus the M type stars from Z91's atlas. We consider EW(CaT) to be zero for stars hotter than 6700 K which is the observational limit of DTT89's atlas.

3.1. Grid I: theoretical fitting functions

JCJ92 computed a complete grid of NLTE models for the equivalent widths of CaT lines from stars with T_{eff} ranging between 4000 and 6600 K, logg between 0.00 and 4.00, and calcium abundances between 0.1 and 1.6 solar. From their models, the following fitting functions can be used to calculate the theoretical value of EW(CaT) as a function of T_{eff} , logg, and calcium abundance, [Ca/H] = -1.0, -0.5, 0.0 and +0.2 (equations (3), (4), (5) and (6) respectively).

$$EW_{-1.0} = -5.03 - 0.136 \log g + 0.304 \log^2 g + 4.18 \cdot 10^{-3} T_{eff} - 4.10 \cdot 10^{-7} T_{eff}^2 - 3.14 \cdot 10^{-4} \log g T_{eff}$$
(3)

$$EW_{-0.5} = -10.28 - 1.83 \log g + 0.493 \log^2 g + 7.46 10^{-3} T_{eff} - 7.08 10^{-7} T_{eff}^2 - 2.20 10^{-4} \log g T_{eff}$$

$$\tag{4}$$

$$EW_{+0.0} = -14.25 - 5.00 \log g + 0.703 \log^2 g + 1.13 \cdot 10^{-2} T_{eff} - 1.09 \cdot 10^{-6} T_{eff}^2$$
(5)

$$EW_{+0.2} = -16.00 - 5.88 \log g + 0.811 \log^2 g + 1.32 \cdot 10^{-2} T_{eff} - 1.27 \cdot 10^{-6} T_{eff}^2$$
(6)

where $EW_{[Ca/H]}$ indicates the value, in Å, of CaT index (sum of the equivalent widths from the two strongest lines, at 8542, 8662 Å), computed with the continuum band-passes located as in DTT89. [Ca/H] means the calcium abundance with respect to the solar value. Conversion between the metallicity Z of the isochrones and the [Ca/H] index of the fitting functions is made adopting Z=0.02 for [Ca/H]=0 and by linearly scaling the index for other metallicies. JCJ92 do not compute theoretical EW(CaT) for metallicities higher than 1.6 solar. We have assumed the use of equation (6) for our calculations at Z=0.05 (2.5 $\rm Z_{\odot}$), and therefore the values of EW(CaT) could be understimated. For metallicities lower than solar a linear interpolation between the values of the indices given by the above expressions has been done.

3.2. Grid II: empirical fitting functions

In the second grid of models we made use of the observational data collected by DTT89 complemented by data of M-late type stars from Z91. DTT89 provide the following relation between EW(CaT), gravity and stellar abundance as measured by [Fe/H]:

$$EW(CaT) = 10.21 - 0.95 \log g + 2.18 [Fe/H] \tag{7}$$

This relation has been adopted for the metallicities Z=0.004 and Z=0.008, assuming [Fe/H]=0 for Z=0.02.

For models with Z=0.02 and Z=0.05, we have fitted the observational data of the EW(CaT) as a function of the gravity, following equations (8) and (9).

$$EW(CaT) = 13.76 - 2.97 \log g \quad ; if \log g < 2$$
 (8)

$$EW(CaT) = 9.51 - 0.78 \log q$$
; if $\log q \ge 2$ (9)

The above relations are shown in Figure 3 a) together with the theoretical calibrations given by JCJ92 for different effective temperatures.

Fig. 3. Comparison between data and models of EW(CaT) in stars. Panel a) shows the EW(CaT) as a function of the gravity. Open circles represent data from DTT89. Solid lines correspond to JCJ92's fitting functions for the values of the effective temperature labelled in the figure. The dotted line is our fit to DTT89's data, which has been used in the models (grid II). Panel b) shows the EW(CaT) as a function of the effective temperature for the coolest stars. For stars cooler than 4000 K, we have extrapolated the expressions given by JCJ92 for stars with T_{eff} between 4000 and 6000 K. Open circles are the data from Z91.

As already anticipated, for M-late stars we adopted the data by Z91, since these stars were not included in DTT89's library. The data given by Z91 have been converted to DTT89's system through the following relation, which has been obtained by fitting a linear regression to 20 common stars in Z91 and DTT89:

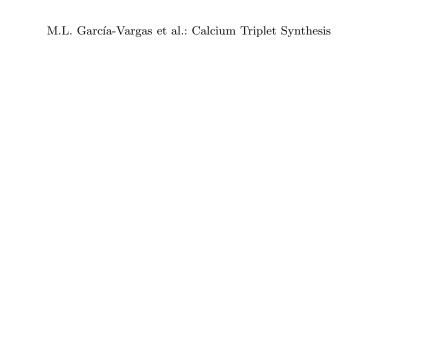
$$EW(DTT89) = (0.87 \pm 0.07)EW(Z91) + (0.70 \pm 0.58); \tag{10}$$

The resulting final expression adopted for M-late stars ($T_{eff} \le 4000 \text{ K}$ and $\log \ge 3.00$) is:

$$EW(CaT) = (6.06 \pm 1.51) \, 10^{-3} T_{eff} - (14.19 \pm 5.31); \tag{11}$$

Figure 3 b) shows Z91's data for M-type stars and JCJ92' models, as a function of the effective temperature. Different curves correspond to models with different gravity as indicated in the plot.

With the above fitting functions we computed the synthetic equivalent widths for the two main lines of CaT at $\lambda\lambda$ 8542,8662 Å at the four selected metallicities: 0.2 Z_{\odot} , 0.4 Z_{\odot} , Z_{\odot} and 2.5 Z_{\odot} . The results are shown in figure 4 and the values are given in tables 3, 4 (grid I), 5 and 6 (grid II). For each table, column (1) lists the logarithm of the age of the SSP (in yr), column (2) the continuum luminosity (in units of L_{\odot}) from the SSP (nebular emission not included), taking an average value in the DTT89's spectral band-passes; column (3) the luminosity, in units of L_{\odot} , absorbed in the Ca II lines at 8542 and 8662 Å by the stars of the SSP, and column (4) the equivalent width of CaT, in Å, computed as the ratio between column (3) and the total continuum luminosity (in which both the stellar and the nebular contribution are taken into account). Columns (5), (6) and (7) are the same of (2), (3) and (4) respectively, but for a different metallicity.



9

Fig. 4. Computed models for the CaT index as a function of the age of the SSP in a logarithmic scale. Panels a), b), c), and d) display the results for metallicities 2.5 Z_{\odot} , Z_{\odot} , 0.4 Z_{\odot} , and 0.2 Z_{\odot} respectively. Solid points correspond to grid I, and therefore based on JCJ92's theoretical calibrations for EW(CaT); and open circles correspond to grid II, based on data from DTT89 and Z91.

4. Discussion

Figure 4 shows the computed values of the CaT for SSPs. At $Z=2.5~Z_{\odot}$ (Fig. 4a) both grids predict similar values of EW(CaT). However, at lower metallicities, the empirical calibration (grid II) provides EW(CaT) that are systematically larger than those computed with the theoretical fitting functions (grid I). For ages older than 100 Myr, the average differences between both grids are 1.2, 1.5 and 2 Å for metallicities Z_{\odot} , 0.4 Z_{\odot} and 0.2 Z_{\odot} respectively.

JCJ92 suggested that the differences found between their models and DTT89's data could be due to the different abundance scale – we must remind that grid I scales the abundances with [Ca/H] since grid II does with [Fe/H] – In the present models, a solar abundance ratio [Ca/Fe] has been assumed, but this could not be the case. In fact, both observations and chemical evolution models show that for low abundances ([Fe/H] \leq -1) the α elements are enhanced with respect to the solar partition. In particular, the behaviour of [Ca/Fe] versus [Fe/H] is shown in Figure 5c from Mollá & Ferrini (1995) for the galactic bulge: [Ca/Fe] keeps constant (\simeq 0.5) for a low [Fe/H] abundance and thereafter it decreases towards the solar value.

The observed enhancement of alpha-elements is due to a lower proportion of iron group elements to alpha-elements at low Z when compared with the corresponding ratio at the solar Z value. In other words, stars of low Z (where Z is representative of alpha-elements) have a lower value of Fe/H than stars with higher Z, as clearly demonstrated by the study of globular clusters. In particular stars with subsolar Z have supersolar abundance ratios. To account for this in the comparison between the observational and predicted values of CaT, we should use stars of lower observed Z than the value of Z used in the theoretical isochrones. At lower metallicities, this effect is larger. We also performed several tests aimed to clarify the role of the $[\alpha / \text{Fe}]$ on the evolution of the star in the HR diagram and they confirmed that isochrones with the same global metallicity Z but a different enhancement of the α elements are almost indistinguishable in the HR diagram (see also Salaris et al. 1993). In summary, to compare both grids, we should use a non solar partition of the heavy elements for abundances lower than solar. The net effect would be a correction in the values of [Fe/H] adopted in equation (7).

The real effect of different [Ca/Fe] ratios has been taken into account by Idiart etal (1997). These authors, by measuring the CaT index in a sample of stars whose [Ca/H] and [Fe/H] were known, found a weak dependence of CaT index with the [Ca/Fe] ratio.

In the galactic star sample used by DTT89 this effect only appears at low metallicity. Therefore it explains the differences between DTT89 and JCJ92 results found in panels c) and d), because the low abundance stars present in DTT89s sample have been used to compute our grid II. However, the same explanation cannot be invoke in the case of solar abundance, panel b), where the partition must be solar for the neighbourhood stars.

The differences found between the two grids in the oldest populations at Z=0.008 could be due to the use, in grid II, of the solar M-late relation, equation (11), also at Z=0.008, producing values of EW(CaT) that could be overestimated. This does not occur in grid I, in which both $T_{\rm eff}$ and abundance dependence are consistently taken into account in the theoretical calibrations. For these reasons we consider grid I more reliable than grid II although, on the other hand, this last one rest on the extrapolation of the JCJ's relation for the coolest stars, for which unfortunately, we have not found observed values either theoretical models.

The above disagreement between the two grids notwithstanding, we may draw the following general conclusions.

At the higher metallicities the EW(CaT) shows a clear maximum around 10 Myr. This is due to the prominence of the RSG phase at these ages and metal content. At earlier stages massive stars evolve according to the O-BSG-WR sequence, while at lower metallicity the scheme followed is O-BSG-YSG-RSG, with the later phase being only a tiny fraction of the total lifetime.

The dependence on metallicity can be easily quantified. Synthetic values of the index higher than 7 Å are only found in models with metallicity Z_{\odot} or higher, reaching values as high as 11 Å only for 2.5 Z_{\odot} models. The variation with the metallicity is due, on one hand, to the intrinsic dependence of the index and, on the other, to the stellar evolution effect just described (see also section 2.1)

From this maximum value the index decreases as the age increases up to a value of about 100 Myr. In the case of the two metal poor sets the index remains almost constant with time up to this age. Around 100 Myr the appearance of the AGB phase produces a sudden increase of the index which then decreases until 1 Gyr. At this stage the advent of the RGB induces another discontinuity which is more evident at the highest metallicity. As the increasing duration of the RGB phase at increasing age is compensated by a decrease of the evolutionary flux of stars and by a shortening of the AGB phase, the integrated value of the index becomes almost age-independent. In clusters older than a few Gyr the metallicity is the dominant parameter driving the integrated value of EW(CaT).

It would be desirable to compare these models with the equivalent widths of clusters at different ages and metallicities (SSP) making use of the same isochrones library.

Fig. 5. EW(CaT) versus [Fe/H]. Filled symbols are data measured in old galactic globular clusters compiled from the literature (Bica & Alloin 1986b, 1987; Armandroff & Da Costa 1991; Armandroff et al. 1992 and Geisler et al. 1995). Open symbols are our two grids of models as labelled in the plot.

The main body of available data is the one from Bica & Alloin (1986a, b) who presented a data-base of star clusters at different ages and metallicities. For the young metal-poor clusters in the Magellanic Clouds, Bica *et al.* (1986, 1990) give also the value of the CaT, but the error bars quoted for the age and metallicity are too large to provide a reliable test for our models.

In the case of old SSPs, for which we have shown that the CaT index is mainly a function of abundance, we have collected in Figure 5 the observed values of the EW(CaT) against [Fe/H] for several globular clusters and we have compared them with the results from our models at an age of 13 Gyr. We must refer our results to [Fe/H] abundance scale. This is the case of grid II. However, since grid I uses [Ca/H], we must account for the enhacement of $[\alpha$ -elements/Fe] as we have explained above. Therefore, we have assigned the value of [Fe/H] for every total abundance Z or [Ca/H] value, by using the [Ca/Fe] relation found by Mollá & Ferrini (1995) already quoted. This relation implies a correction of 0.0, -0.2 and -0.4 dex for values of [Ca/H] solar, 0.4 solar and 0.2 solar respectively.

Data in Figure 5 shows that in old systems a narrow correlation between the CaT index and the metallicity over more than two orders of magnitude in [Fe/H] is found and, at the same time, they provide a significant reliability test for the theoretical models presented here.

Finally, a recent paper by Mayya (1997) presents CaT synthesis models to be applied to starburst regions. Therefore only young population results may be compared with our models. Mayya uses JCJ92 fitting functions for $Z \le Z_{\odot}$ and DTT89 empirical relations for higher metallicities. He uses the stellar evolutionary tracks from Geneva group. His results also show a primary peak due to the RSG phase, a secondary maximum and a low constant value for SSP older than 100 Myr. Both peaks occur at earlier ages than in our models, due to differences in the assumed stellar tracks, and the asymptotic value is lower than the one in our grid II. The most important difference appears at lower abundances: at Z=0.008 the first maximum disappears in our models, while it exists in Mayya's. The evolutionary tracks selected by Mayya (1997) with enhaced mass loss rates for low abundances produce this behaviour, not predicted with the Padova evolutionary models either previous generation of Geneve tracks. The convenience of the use of these enhanced mass loss rates is still a matter of debate.

4.1. CaT synthesis in composite-populations: unveiling the presence of RSG in star-forming regions

CaT has been observed not only in star clusters and normal galaxies but also in Active Galaxies (Terlevich et al. 1990a; Nelson & Whittle 1995; Palacios et al. 1997) and star-forming regions like Starbursts (Terlevich et al. 1990a, b; García-Vargas et al. 1993; González-Delgado et al. 1995) and Giant Extragalactic HII Regions, GEHRs, (Pastoriza et al. 1993; González-Delgado et al. 1995; Terlevich et al. 1996).

There is a controversy related to the origin of the observed CaT in star-forming regions and AGNmostly because these regions are not spatially resolved from the ground. Therefore one of the key questions is if the observed CaT comes from a single stellar population RSG rich or from a result of a mixture of populations of varying age and possibly metallicity (including the RSG plus the underlying older population).

In the case of isolated GEHRs, and therefore not contaminated by an underlying old population, two possibilities can arise: (1) the production of the CaT is due to the same young burst that is ionizing the region and (2) the CaT is produced in a slightly older (10-15 Myr) population, coexisting in the same GEHR with the younger, ionizing, one. With respect to the first scenario, current theoretical models (Salasnich et al. 1997) predict a narrow range of age and metallicity in which an SSP can produce both ionizing stars (O and WR stars) and RSG, namely around 4-6 Myr and at solar metallicity. This has been proposed for the CaT observations in NGC 604 (Terlevich et al. 1996). However, some other GEHR need the existence of an older component, second scenario, such is the case of some GEHR in the circumnuclear region of NGC7714 (García-Vargas et al. 1997).

The largest circumnuclear GEHRs usually show the CaT feature in their spectra. However, some contamination from the older underlying population in the host galaxy is expected and therefore it is not clear whether the CaT is originated in the GEHR or in the disk-bulge population (García-Vargas et al. 1997).

In the case of starburst galaxies and AGN the picture is even more difficult to interpret, and the need for models which include the CaT synthesis from different populations becomes a key issue. To study this problem we have computed composite models with a combination of three different kind of populations: (a) a young one, able to ionize the gas, and definitively present in the region, (b) an intermediate age one, RSG rich, and (c) a very old population representative of those present in ellipticals and bulges of spirals. The selected ages are, 2.5 and 5 Myr for the youngest population, 8 and 12 Myr for the intermediate component and 10 Gyr for the oldest one. Three types of models have been computed: (1) a combination of two coexisting bursts, young, and intermediate, contributing 50 % each in mass, suitable to be used in GEHRs, without any underlying population; (2) a two-component model in which the young burst plus the old population are combined in different proportions, and (3) a three-component model in which two coexisting bursts, young and intermediate-age, plus the old underlying population are contributing to the light in different percentages. The metallicity of the old population has been chosen to be Z_{\odot} , 0.4 Z_{\odot} and 0.2 Z_{\odot} for young populations with 2.5 Z_{\odot} , Z_{\odot} and 0.4 Z_{\odot} respectively, according to what is predicted by chemical evolution models.

To define the relative proportions we use the ratio, P, of the continuum luminosity at 6500 Å (close to H_{α}) of the young and intermediate population (when present) to the total light. As an example P = 0.10 indicates a model in which the population characteristic of the region (young or young + intermediate) is contributing 10 % to the total light in the continuum at H_{α} . This method allows a check of the adopted proportions by a direct inspection of the H_{α} images. We have computed models with P ranging from the ones typical of GEHRs (P = 0.10 - 1 going from the smallest to the largest regions) to the ones characteristic of the most powerful starburst galaxies (P= 1 - 100).

Tables 7, 8 (grid I) 9 and 10 (grid II) display the results of the composite-population models. Each table contains the results for three metallicities: $0.4 \, \mathrm{Z}_{\odot}$, Z_{\odot} and $2.5 \, \mathrm{Z}_{\odot}$. The first column lists the proportion, P, defined above (including the two – tables 7, 9 — or three — tables 8, 10 — populations considered). If P is not given, a single population, or a combination of two coexisting young populations contributing 50 % in mass each, have been considered. Column 2 shows the age of the population(s), in Myr. Therefore $2.5 + 10^4$ correspond to a model in which a young burst of 2.5 Myr is combined with an old population of 10 Gyr. Column 3, EW(CaT), lists the value of the equivalent width of CaT in absorption, in Å, for each model. Finally column 4 is the equivalent width of H_{β} Balmer line in emission. If this value is missing then the adopted population(s) is(are) too old to produce ionizing photons.

The predicted values of $EW(H_{\beta})$ in emission have been computed without considering the dust associated to the ionized region. There exists a well known discrepancy between predicted and observed values of $EW(H_{\beta})$ (e.g. Viallefond & Goss 1986). In fact, only 3 out of 425 HII galaxies in the catalogue by Terlevich *et al.* (1991) show $EW(H_{\beta})$ comparable to the ones calculated for clusters younger than about 3 Myr (i.e. > 350 Å; Mas-Hesse & Kunth 1991; García-Vargas *et al.* 1995a; Stasińska & Leitherer 1996). Under the assumption of a single burst population and a radiation bound nebula, an explanation for this disagreement could be that the reddening affecting the emission lines is caused by dust inside the regions (associated to the gas) which therefore does not affect the continuum of the ionizing cluster (Mayya & Prabhu 1996). If this is the case, the measured $EW(H_{\beta})$ should be increased according to

the reddening determined from the emission lines and taking into account the contribution of the nebular continuum (García-Vargas et al. 1997).

Columns 5, 6 (Z_{\odot}) and 7, 8 (0.4 Z_{\odot}) contain the same as columns 3, 4 already described for the case of 2.5 Z_{\odot} . To summarize the results, we plot in Figure 6 the value of EW(CaT) against that of EW(H_{\beta}). This figure can be used as a diagnostic diagram to unveil the presence of an intermediate population RSG rich, when analyzing data of star-forming regions which are located over an older underlying population. This is usually the case of AGN, nuclear starbursts and circumnuclear GEHRs. The results for the grid I are divided in in four panels. These panels simulate four different types of star-forming regions: a)AGN, corresponding to solar metallicity and large P values, b) circumnuclear high metallicity HII regions with solar metallicity but low P values, c) nuclear starbursts having half solar metallicity and high P, and d) circumnuclear GEHR with moderate metallicity (0.4 Z_{\odot}) and low P values.

Inspection of tables 7, 8 and Figure 6 shows that for powerful starburst galaxies (with values of P larger than 1.00) values of EW(CaT) higher than 3.8 Å are predicted only if RSG are present in the region and, in this case, the two-component models (ionizing burst+bulge) would not be able to reproduce the observations. García-Vargas et al. (1993) gave values of CaT in starbursts ranging between 2.5 and 8 Å. As can be seen in Figure 6 c) a value as low as 2.5 Å can imply a low metallicity, an older age or simply the absence of RSG, and only a detailed study of other observational constraints could provide the solution. On the contrary, values as high as 8 Å would necessarily imply the presence of RSG and a metallicity at least solar, therefore somewhat higher than the average metallicity found in starburst galaxies.

The same method can be applied to AGN. In this case, a detection of CaT higher than 5 Å implies the presence of RSG inside the region sampled by the slit, probably larger than the nucleus and including also the subarcsec circumnuclear rings as shown by HST observations of some of the nearest AGN (Colina et al. 1997). Terlevich et al. (1990a) showed that all AGN in their sample had values of $EW(CaT) \ge 5$ Å, therefore implying the presence of RSG.

In the case of circumnuclear GEHRs the discrimination between the presence or absence of RSG is a difficult task, particularly at moderate metallicity (see Fig6b and 6d). A more detailed study with further observational constraints is needed to discriminate between the two possibilities, such as the analysis of the whole optical spectrum to constrain the age of the young burst and an image near H_{α} to determine P (García-Vargas et al. 1997)

4.2. CaT in old populations: a strong metallicity constraint

We now turn to old populations, namely elliptical galaxies and bulges of spirals. Terlevich et al. (1990a) present a sample of 14 objects, whose EW(CaT) are between 6.1 and 8.1 Å (typical error bar of \pm 0.8 Å) measured as in DTT89 and thus directly comparable to our models. Delisle & Hardy (1992) give central values (and also gradients) for 12 galaxies, with CaT equivalent widths ranging between 6.4 and 7.7 Å (typical error bar of \pm 0.2 Å). In spite of different spectral band-passes than DTT89, but also free from TiO bands contamination, the comparison of three common objects, M 31, M 81 and NGC 1700, gives values of 6.4, 7.3 and 7.0 Å in Delisle & Hardy (1992) and 6.1, 7.7 and 6.1 in Terlevich et al. (1990a) respectively, which are consistent within the errors. In summary the available observed values of the CaT index in old populations (elliptical and bulges of spirals) are between 6 and 8 Å. These numbers compare well with our old SSP models of solar metallicity (Fig. 4b) and suggest a quite uniform average metallicity for these systems in agreement with what is derived by detailed galactic models of narrow band indices (Bressan et al. 1996).

Vazdekis et al. (1996, V96) compute evolutionary synthesis models for early-type galaxies, with metallicities $0.4~\rm Z_{\odot},~\rm Z_{\odot}$, and $2.5~\rm Z_{\odot}$ and ages 1, 4, 8, 12 and 17 Gyr. They consider different hypotheses about the IMF, the chemical evolution and the star formation history, producing a set of models which includes colours and line indices, in particular CaT. Since the evolutionary scheme is the same that the one assumed in our models, we present in Table 11 a comparison between V96 models and our grid II for the SSP with common ages and metallicities.

V96 give values higher than grid II at Z=0.02 and 0.05, and lower at Z=0.008 (except at 1 Gyr). For the highest metallicty, a source of the discrepancy could be the different assumed fitting function for the index (although both based on DTT89, they use a single fit for any abundance, as in DTT89, since we use equations 8 and 9 for Z_{\odot} and 2.5 Z_{\odot} . The rest should be due to the inclusion in our models of the coolest late-type stars, Z91, and therefore a different modelization of CaT index for cool stars, important in old populations. This comparison stress the need of observations of cool stars to test the present calibratios.

Idiart etal (1997) also compute synthetic values of CaT in old populations. They use a calibration based on their own star sample, with a different index definition, which includes the three calcium lines. They also include in their models late-type stars from Z91 but not high metallicity RSG stars (although these stars are not present in such old populations, the lack of high metallicity RSG in their star sample implies that their values would be definitively lower than ours in RSG-rich populations at metallicities solar or higher than solar). In the range-age (1-12 Gyr) in which we can compare our models with Idiart's, their resulting EW(CaT) for SSP are slightly lower than those from our



Table 11. Comparison between V96 and grid II for old populations

Z	Model	1 Gyr	4 Gyr	8 Gyr	12 Gyr	17 Gyr
0.008	V96	6.24	6.63	6.79	6.88	6.97
0.008	grid II	5.78	7.21	7.31	7.43	7.48
0.02	V96	8.32	8.44	8.25	8.22	8.09
0.02	grid II	6.84	8.57	8.57	8.63	8.57
0.05	V96	8.50	8.90	8.34	8.08	7.92
0.05	grid II	7.22	9.92	9.62	9.65	9.63

grid II models. However, the values agree quite well (as an example, at $0.3~\rm Z_{\odot}$ their values are $5.53~\rm and~6.50~\rm Å$ for populations at 1 Gyr and 12 Gyr, since ours (as calculated as an average value of $0.2~\rm and~0.4~\rm Z_{\odot}$) are $5.69~\rm and~7.19~\rm Å$ respectively. At $\rm Z_{\odot}$ Idiart's values are $6.57~\rm and~7.55~\rm Å$ again for the extreme ages 1 Gyr and 12 Gyr, since ours are $6.84~\rm and~8.60~\rm Å$ at the same ages. Differences can come not only from the calculations in the CaT index but from the different assumptions adopted in the low-mass limit of the IMF and in the evolution of the low-mass stars.

An important point is the relatively low sensitivity of the CaT index to the age above a few Gyr, makes it a very powerful tool for discriminating among the metallicity of the stellar systems. It is well known that due to the similar response of the isochrone turn-off to variations in age or metallicity it is difficult to disentangle age and metallicity effects by the sole analysis of the integrated properties of the spectra in old populations. Different diagnostic diagrams have been adopted, as can be seen in González (1993) and Bressan et al. (1996) none of which is fully adequate to overcome this difficulty. The quantity

$$\frac{\delta logCaT/\delta(logage)}{\delta logCaT/\delta logZ} \tag{12}$$

is a measure of the relative sensitivity to age and metallicity. At t=13 Gyr and Z= Z_{\odot} this quantity is 2.876, but the average value between 2 and 13 Gyr is 6.4. Among the narrow band indices considered so far in the literature (Gorgas et al. 1993, Worthey et al. 1994, Bressan et al. 1996) this is the one with the highest sensitivity to the metall content. Jones & Worthey (1995) claimed that the Fe₄₆₆₈ index has a large sensitivity to the metallicity with a value δ (log age)/ δ (log Z)=4.9, that is lower than our mean result of 6.4. These same authors use the index $H_{\gamma_{HR}}$ as an age discriminator, due to its total independence of the metallicity: δ (log age)/ δ (log Z)=0.0. We have not calculated it, but a suitable combination of the CaT index with another whose age sensitivity is higher, such as the H_{β} index (the following one with low sensitivity to the metallicity with a δ (log age)/ δ (log Z)=0.6, could definitively separate age from metallicity and solve the age-metallicity dilemma in early-type galaxies (Bressan et al. 1996). Thus, as a preliminary step and awaiting for our own complete galaxy models, we can generate mixed diagnostic diagrams using our models for CaT index and the narrow band indices from Bressan et al. (1996), that are computed adopting the same library of stellar evolutionary tracks.

Figure 7 shows the synthetic values of the EW(CaT) plotted against the logarithm of H_{β} index as modelled by Bressan *et al.* (1996). It can be seen that curves of constant age are almost orthogonal to curves of constant metallicity, making this diagram one of the most powerful tools to solve the problem of the age-metallicity degeneracy in elliptical galaxies in a similar way to Figure 2 from Jones & Worthey (1995).

Although more theoretical work has to be made to assess the importance of the study of CaT in old systems, the use of the later index as a straightforward metallicity indicator in early-type galaxies is very promising (Gorgas *et al.* 1997).

5. Conclusions

Models for CaT index have been computed for SSP ranging in age from 1 Myr to 17 Gyr and in metallicity from 0.2 to $2.5 \, \mathrm{Z}_{\odot}$ in order to evaluate the usefulness of this index to constrain the age and metallicity of stellar populations. Two grids of models have been generated, based on different calibrations of the index as a function of the stellar parameters: effective temperature, gravity and abundance: grid I assumes the theoretical calibration given by JCJ92 and grid II a fitting to observational data (DTT89, Z91). Values from grid I are systematically lower than those from grid II. Since the abundance scale is different in the two set of models, [Ca/H] in grid I, [Fe/H] in grid II, the differences at low

Fig. 7. EW(CaT) (grid I, this work) versus the computed values for the logarithm of H_{β} index (Bressan *et al.* 1996) in old populations.

metallicity can be explained if an enhacement of α elements, like Ca, with respect to the solar partition is assumed. When cool M-type stars are present in a SSP, the different calibration assumed in both grids leads to different values for CaT, and more data and models are needed to account properly for the contribution of these stars to the index.

The evolution of EW(CaT) in SSP with time presents a primary maximum when RSG appear (around 10 Myr). The value of this peak is strong metallicity-dependent due to both, the evolutionary tracks and the intrinsic dependence of the index with the abundance for supergiants. At about 100 Myr the appearance of the AGB phase produces a sudden increase of the index (secondary maximum) followed by a decrease until 1 Gyr, remaining then almost constant for a given metallicity.

In star-forming regions, we propose the use of a diagnostic diagram, EW(CaT) versus EW(H_{β}) in emission, to evaluate if CaT is produced by RSG in the region, or by an underlying old population and therefore as a tool to date the starburst. This diagnostic is a powerful indicator of the presence of RSG in high metallicity scenarios, where values larger than 4-5 Å unveil the presence of young RSG. At lower metallicities, the sole use of the diagram cannot disentangle between giant and RSG contributions, especially if the starburst is not very luminous with respect to the underlying population.

Finally, the behaviour of the index in populations older than 1 Gyr shows that the strength of CaT index is controlled by the abundance, leading us to propose another diagnostic diagram, this time using EW(CaT) versus the logarithm of the traditionally used H_{β} (absorption) index, as a tool to break the age-metallicity degeneracy in elliptical galaxies.

More theoretical work and observed data are needed to assess the importance of CaT for abundance and age determination in stellar populations.

Acknowledgements. We thank Javier Gorgas, Enrique Pérez , Rosa González-Delgado, Eduardo Hardy and Claus Leitherer for their helpful comments. This work has been partially supported by the Spanish DGICYT project PB 93-052 and by the TMR grant ERBFMRX-CT96-0086 from the European Community. We also thank the anonymous referee for the useful comments which have contributed significatively to the improvement of the paper. Finally, we thank N. Smith for her help with English during the revision of the manuscript.

References

Aller L.H., 1984, Physics of Thermal Gaseous Nebulae (Dordrecht: Reidel), 102

Armandroff T.E. & Da Costa G.S., 1991, AJ, 101, 1329

Armandroff T.E., Da Costa G.S. & Zinn R., 1992, AJ, 104, 164

Bertelli G., Bressan A., Chiosi C., Fagotto F. & Nasi E., 1994, A&AS, 106, 275

Bica E. & Alloin D., 1986a, A&AS, 66, 171

Bica E. & Alloin D., 1986b, A&A, 162, 21

Bica E. & Alloin D., 1987, A&A, 186, 49

Bica E., Dottori H. & Pastoriza M., 1986, A&A, 156, 261

Bica E., Alloin D. & Santos J.F.C., 1990, A&A, 235, 103

Bressan A., 1994, Space Science Reviews, 66, 373

Bressan A., Fagotto F., Bertelli G., & Chiosi C., 1993, A&AS, 100, 647

Bressan A., Chiosi C. & Tantalo R. 1996, A&A, 311, 425

Chiosi C., Bertelli G. & Bressan A., 1992, ARA&A, 30, 305

Clegg R.E.S. & Middlemass D., 1987, MNRAS, 228, 759

Colina L., García-Vargas M.L., Mas-Hesse M., Alberdi A. & Krabbe A., 1997, ApJL, 484, 41

Danks A.C. & Dennefeld M., 1994, PASP, 106, 382

de Jager C., Nieuwenhuijzen H. & van der Hucht K. A., 1988, A&AS, 72, 259

Delisle S. & Hardy E., 1992, AJ, 103, 711

Deng L., Bressan A. & Chiosi C., 1996, A&A 313, 145

Díaz A.I., Terlevich E. & Terlevich R., 1989, MNRAS, 239, 325, DTT89

Erdelyi-Mendes M. & Barbuy B., 1991, A&A, 241, 176

Fagotto F., Bressan A., Bertelli G. & Chiosi C., 1994a, A&AS, 104, 365

Fagotto F., Bressan A., Bertelli G. & Chiosi C., 1994b, A&AS, 105, 29

Feast, M. W. 1992, in "Instabilities in Evolved Super and Hypergiants", ed. C. de Jager, H. Nieuwenhuijzen, Amsterdam, North Holland p. 18

Ferland G.J., 1980, PASP, 92, 596

García-Vargas M.L., 1996, From Stars to Galaxies: the impact of stellar physics on galaxy evolution, PASP Conference Series, vol 98, p. 244.

García-Vargas M.L., Díaz A.I, Terlevich E. & Terlevich R., 1993, A&SS, 205, 85

García-Vargas M.L., Bressan A. & Díaz, 1995a, A&AS, 112, 13

García-Vargas M.L., Bressan A. & Díaz, 1995b, A&AS, 112, 35

García-Vargas M.L., González-Delgado R.M., Pérez E., Alloin D., Díaz A.I & Terlevich E., 1997, ApJ, 478, 112

Geisler D., Piatti A.E., Clariá J.J. & Minnitti D., 1995, AJ, 109, 605

González-Delgado R.M, Pérez E., Díaz A.I., García-Vargas M.L., Terlevich E. & Vílchez J.M., 1995, ApJ, 439, 604

González J.J., 1993, PhD Thesis, University of California, Santa Cruz.

Gorgas J., Faber S.M., Burstein D., González J.J., Courteau S. & Prosser C., 1993, ApJS, 86, 153

Gorgas J., García-Vargas M.L., Cardiel N., Mollá M. & Bressan A., 1997, in preparation

Idiart T.P, Thévenin F. & De Freitas Pacheco J.A., 1997, AJ, 113, 1066

Iglesias C.A., Rogers F.J., & Wilson B.G., 1992, ApJ, 397, 717

Jones J.E., Alloin D.M. & Jones B.J.T., 1984, ApJ 283, 457

Jones L.A. & Worthey G., 1995, ApJL, 446, 31

Jørgensen U.G., Carlsson M. & Johnson H.R., 1992, A&A, 254, 258, JCJ92

Kurucz R., 1992, Precision Photometry: Astrophysics of the Galaxy, ed. P.G. Davis Philip, A.R. Upgren & K.A. Janes, L.Davis press, Schenectady

Langer N., 1989, A&A, 210, 93

Maeder A. & Conti P., 1995, ARA&A, 32, 227

Mallik S.V., 1994, A&AS, 103, 279

Mas-Hesse, J.M. & Kunth, D., 1991, A&AS, 88, 399

Mayya, Y.D., 1997, ApJL, 482, 149

Mayya, Y.D. & Prabhu, T.P., 1996, AJ, 111, 1252

Mollá M. & Ferrini F., 1995, ApJ, 454, 726

Nelson C.H. & Whittle M., 1995, ApJS, 99, 67

Palacios J., García-Vargas M.L., Díaz A.I., Terlevich R. & Terlevich E., 1997, A&A, in press

Pastoriza M.G., Dottori H.A., Terlevich E., Terlevich R. & Díaz A.I., 1993, MNRAS, 260, 177

Salaris M., Chieffi A. & Straniero O., 1993, ApJ, 414, 580.

Salasnich B., Bressan A. & Chiosi C., 1997, Diffusion and mass loss in massive stars in Fundamental Stellar Properties: the Interaction between Observation and Theory, IAU Symposium 189, Sydney, Australia.

Salpeter E.E, 1955, ApJ, 121, 161

Smith G. & Drake J.J., 1987, A&A, 181, 103

Smith G. & Drake J.J., 1990, A&A, 231, 125

Stasińska, G. & Leitherer, C. 1996, ApJS, 107, 661

Terlevich E., Díaz A.I. & Terlevich R., 1990a, MNRAS, 242, 271

Terlevich E., Díaz A.I., Pastoriza M.G. & Terlevich R., 1990b, MNRAS, 242, 48_P

Terlevich R., Melnick J., Masegosa J., Moles M. & Copetti M.V.F. 1991, A&AS, 91, 285

Terlevich E., Díaz A.I., Terlevich R., González-Delgado R.M., Pérez E. & García-Vargas M.L., 1996, MNRAS, 279, 1219

Vazdekis A., Casuso E., Peletier R.F. & Beckman J.E., 1996, ApJS, 106, 307

Viallefond, F. & Goss, W.M. 1986, A&A, 154, 357

Worthey G., Faber S.M., González J.J. & Burstein D., 1994, ApJS, 94, 687

Zhou X., 1991, A&A, 248, 367, Z91

